# Chapter 4
# Energy-Based Assessment of Commercial Adaptive Cruise Control Systems

**Theocharis Apostolakis** ⓘ**, Michail A. Makridis** ⓘ**, Anastasios Kouvelas** ⓘ**, and Konstantinos Ampountolas** ⓘ

**Abstract** Vehicle automation is regarded as one of the most promising technologies in transportation networks to alleviate congestion, improve safety and energy efficiency. Adaptive cruise control (ACC) systems, which serve as the first step of automation, are already standard equipment in many commercially available vehicles. Therefore, the observation-based assessment of such systems individually and in platoon formations is very appealing. The thematic focus of this study is laid on investigations into the impact of ACC systems on energy and fuel consumption inside the platoon. High-resolution data from two experimental car-following campaigns consisted of platoons with ACC-equipped vehicles are collected. Two driving modes are considered, human- and ACC-driven vehicles. Results are presented with four independent energy consumption models. The findings reveal that an upstream energy propagation was observed inside the platoon by the ACC participants, indicating that ACC systems are less efficient than human drivers. On the positive side, ACC systems do not generally fail inside a platoon, keeping steady time-gaps. They seem to operate based on a constant headway policy, and their performance is conditioned to the environment. ACC drivers in protected environments and campaigns might perform better but should be (ideally) tested in adverse environments.

**Keywords** Adaptive cruise control · Tractive energy consumption · Fuel consumption · Experimental campaigns · Driving behavior · Platoon

Th. Apostolakis (✉) · K. Ampountolas
Department of Mechanical Engineering, University of Thessaly, 38334 Volos, Greece
e-mail: tapostolakis@uth.gr

M. A. Makridis · A. Kouvelas
Institute for Transport Planning and Systems, ETH, Zürich, Switzerland

## 4.1   Introduction

The energy and environmental challenges facing humanity are further exacerbated by the rising transport of goods and people. The transport sector is heavily reliant on fossil fuels. As a result, transportation generates a large share of greenhouse gas (GHG) emissions around the world. However, the future of transportation networks is expected to be transformed radically, due to the recent advances in vehicle automation and communication systems. Vehicle automation comes with the promise to increase road safety, road capacity, and traffic flow that are currently limited due to heterogeneity in vehicle dynamics and human driving behaviors. Nowadays, many commercially available vehicles are equipped with advanced driver assistance systems (ADAS) that support the driver by taking over particular driving tasks.

Adaptive cruise control (ACC) systems, which are considered as the first step of driving automation (Level-1 of SAE levels of driving automation [1]), are already optional or standard equipment in many commercially available vehicles. Driving automation of Level-1 undertakes the steering or brake/acceleration task of the driver. Level-2 assumes a combination of multiple assistance functionalities, e.g., undertaking both steering and brake/acceleration tasks of the driver. The ACC system controls the longitudinal movement of the equipped vehicle by monitoring the speed and distance from the vehicle ahead constrained by a user-defined desired speed. ACC uses onboard sensors (right and left side on the front bumper), such as LiDAR, radar, or cameras to continuously detect the distance to the preceding vehicle. ACC can be enabled and disabled by the driver upon request. The driver activates ACC by setting the desired maximum speed and by selecting among different time-gap settings from the preceding vehicle. Then, ACC can automatically adjust the vehicle's speed by accelerating or decelerating it, to maintain a constant predefined headway with the vehicle in front or to reach the predefined desired speed. Moreover, a braking guard can warn about imminent collision and automatically start braking and disengage ACC. ACC disengagement occurs whether the headway between two vehicles is close to infinity or when a vehicle travels with the minimum ACC operating speed. The driving behavioral properties of ACC are considered to reduce heterogeneity, affecting traffic flow (negative or positive depending on the conditions) and affecting fuel consumption and emission pollutants.

The penetration rate of ACC-equipped vehicles on public roads is rapidly increasing, gaining traction among car manufacturers and consumers. However, the surging acceptance of such systems across the globe is escalating concerns on undesired properties of commercial ACC systems such as string instability, negative impact on-road capacity, safety concerns, energy demand, and fuel consumption [2–6].

Studies on the energy footprint of ACC-equipped vehicles are based on traffic simulation or empirical data obtained from experimental campaigns. For instance, a novel vehicular ACC system was proposed that can comprehensively address issues of tracking capability, fuel economy, and driver desired response [7]. Detailed simulations with a heavy-duty truck showed that the developed ACC system provides

significant benefits in terms of fuel economy, achieving fuel savings of 5.9 and 2.2% during urban and highway driving scenarios, respectively.

A large-scale study with a fleet of 51 test vehicles over 62 days and 199,300 miles (driven by General Motor employees on their daily commutes) was conducted to analyze the GHG emissions benefit of ACC from a statistical perspective [8]. The results show that ACC driving could significantly reduce GHG emissions at low speeds, which, however, would hardly deliver a meaningful benefit for the whole journey because ACC utilization rates at low speeds were marginal and low-speed driving only covered a small portion of the total travel distance. Generally, the study reports a positive total GHG (directly correlated to fuel consumption) emissions benefit of the ACC systems.

An experimental campaign involving 10 commercially available ACC-equipped vehicles was presented [9]. The test campaign was executed in two different test tracks of the ZalaZONE proving ground, in Hungary. Results confirm the previous findings in terms of string instability of the ACC and highlight that in the present form, ACC systems may lead to higher energy consumption and introduce new safety risks when their penetration in the fleet increases.

Another field experiment was conducted with seven commercial SAE Level-2 equipped vehicles, driven as a platoon on public roads for a trip of almost 500 km [10]. The study concludes that SAE Level-2 systems are not suitable for driving as platoons of more than typically three to four vehicles, because of instabilities in the car-following behavior and hence, discomfort and large fuel consumption. Finally, another experiment was performed with ACC-equipped vehicles in real-world car-following scenarios from Ispra to Vicolungo and back, in Italy [11]. Two driving modes were adopted, with and without ACC systems enabled. The results show that from individual and platoon perspectives, ACC followers tend to have energy consumption higher than those of human counterparts, questioning the positive impact of ACC systems on fuel and energy consumption.

Experimental observations with partially or fully automated vehicles are scarce, but their number is expected to increase in the coming years due to the availability of heterogeneous, precise, and inexpensive sensors. Nevertheless, the energy demand of automated vehicles, as well as their commonalities and differences with human drivers are not widely discussed in the literature, which constitutes a gap that this work aims to fill. Toward this goal, the present chapter provides a comprehensive study of the energy impact of ACC systems under car-following conditions, based on empirical observations from two independent real-life experimental campaigns, with platoons of ACC-equipped vehicles, using two different data acquisition methods. Their energy impact is assessed by four state-of-the-art energy demand and fuel consumption models available in the literature. Both ACC- and human-driven vehicles are considered in the investigation to elaborate on the behavioral similarities and differences between these two driving modes. As a result, it expands the discussion from safety concerns and technological aspects of ACC systems and includes the effect of transportation on the environment under real circumstances.

The main findings of this work are as follows: (a) In both experimental campaigns, an upstream energy propagation was observed inside the platoon by the ACC participants, regarding both tractive energy and fuel consumption, indicating that ACC systems are less efficient; (b) ACC driving operation (strong accelerations, steep speeds) may negatively affect the energy impact of ACC systems; (c) ACC systems may lead to string instability failing to avoid an upstream energy amplification; and (d) road gradient changes could create string instabilities in the traffic flow and may negatively affect the energy impact of ACC systems.

Despite the above shortcomings of ACC, we highlight that ACC systems do not generally fail inside a platoon, and they drive very steady in equilibrium conditions. Especially on highways, commercially implemented ACC systems can be reliable, safe, comfortable (no need to press the pedal), and energy efficient in equilibrium conditions. To support the above arguments, we show that the time- and space-gaps of the ACC participants are smaller (in absolute values) and better distributed when compared to their human counterparts. This highlights the ability of the ACC drivers to keep constant time-gap policies. We also show that the more efficient ACC systems are regarding their functional specifications, the less energy efficient tend to be. Consequently, commercially implemented ACC systems must be optimized to realize a trade-off between functional specifications in terms of time-gap policies and safe and eco-driving instructions. This will ideally eliminate high energy levels and achieve the desired eco-driving and safety features of commercial ACC systems.

The rest of this chapter is organized as follows: Sect. 4.2 presents four independent energy and fuel consumption models. Two experimental car-following campaigns in Italy and Sweden are then presented, providing us with two large datasets, valuable for the assessment of the four models. Section 4.3 first analyzes the experimental data from the two test campaigns. Then, it assesses the energy footprint of ACC and human drivers as obtained from the application to the considered energy demand and fuel consumption models. Also, it offers a discussion around the similarities and differences between these two driving modes concerning several technical aspects. Specifically, ACC and human driving behaviors are compared with respect to the transient response of speed and acceleration profiles, traffic perturbation events, string stability, and time-gap policies. Finally, Sect. 4.4 summarizes the findings of this study and offers suggestions for future work.

## 4.2 Methodology

This section presents four independent energy and fuel consumption models. The first model concerns the tractive energy consumption [11, 12], ruling out the effect of the propulsion system (tractive power demand on the wheels). The other three models, namely VT-micro [13], VSP [14, 15], and ARRB [16], focus on the (instantaneous) fuel consumption.

## 4.2.1  Tractive Energy Consumption

Tractive energy consumption serves as a suitable indicator for the assessment of ACC driving behavior. This indicator considers only the tractive power demand on the wheels, without considering the powertrain dynamics and the regenerative braking power. Although it does not directly reflect the engine fuel consumption (which will be considered in Sect. 2.2) or the battery charge depletion, this metric can rule out the energy effect of heterogeneous propulsion systems in the traffic network [11].

The instantaneous tractive power ($P_t$, kW) required to move the engine at the defined velocity and surpass the aerodynamic and rolling resistances is given by [12]:

$$P_t = \begin{cases} \left( F_0 + F_1 v_e + F_2 v_e^2 + 1.03 m a_e + mg \cdot \sin\theta \right) v_e \cdot 10^{-3}, & P_t \geq 0 \\ 0, & P_t < 0 \end{cases}, \quad (4.1)$$

where $F_0$, $F_1$, and $F_2$ are road load coefficients that describe the relationship between overall resistances to motion and the vehicle speed, given in N, Ns/m, and Ns$^2$/m$^2$, respectively; m is the vehicle mass (kg); $v_e$ and $a_e$ are the ego vehicle's speed (m/s) and acceleration (m/s$^2$), respectively; $\theta$ is the road gradient (rad); g is the gravitational acceleration (9.81 m/s$^2$).

The terms inside the parentheses in Eq. 4.1 represent the resistance forces to vehicle motion and speed. The $F_0$, $F_1$, and $F_2$ coefficients are commonly used to characterize the road loads of vehicles, as mentioned above. They express the constant part of a vehicle's resistances (tire rolling resistances), the part that is proportional to velocity (partly tire rolling resistance, partly drivetrain losses), and the part that is proportional to the square of the vehicle's velocity (aerodynamic component) [17]. Consequently, the first two terms ($F_0 + F_1 v_e$) represent the rolling resistance force, the second one ($F_2 v_e^2$) the aerodynamic drag, the third term (1.03m$a_e$) is the force of inertia, where the factor of 1.03 is applied to correct the inertia of the vehicle which accounts for the vehicle mass and the inertia of its rotating components, and the last one (mg · sin$\theta$) is related to the force due to gravity and roadway grade.

The vehicle's tractive energy consumption ($E_t$, kWh/100 km) results by integrating the instantaneous tractive power requirements ($P_t$, kW) at the wheels over time, without considering the negative power components from the regenerative braking, and dividing it by the distance covered which corresponds to the integration of the instantaneous speed over time [11]. Finally, a factor of 0.036 is applied to the denominator so that the results are available in the commonly used units mentioned above (kWh/100 km), as described by:

$$E_t = \frac{\int_0^T P_t dt}{0.036 \cdot \int_0^T v_e dt}, \quad (4.2)$$

where $dt$ is the time interval (s) between consecutive measurement points and $T$ denotes the total duration (s) of the travel period.

## 4.2.2   Fuel Consumption

The impact of ACC driving behavior on fuel consumption is assessed with three state-of-the-art vehicle fuel consumption models, namely VT-micro [13], VSP [15], and ARRB [16], focusing on instantaneous fuel consumption.

### 4.2.2.1   The VT-Micro Model

Virginia Tech (VT)-micro model is a microscopic dynamic emission and fuel consumption model [13]. The VT-micro model was developed from experimentation with numerous polynomial combinations of speed and acceleration profiles, on a second-by-second basis [18]. Specifically, linear, quadratic, cubic, and quartic speed and acceleration terms were tested using chassis dynamometer data, collected at the Oak Ridge National Laboratory (ORNL). The ORNL data consisted of nine normal-emitting vehicles, including six light-duty automobiles and three light-duty trucks. The raw data collected at the (ORNL) contained 1300–1600 individual vehicle data points, each collected every second during various driving cycles. Typically, vehicle acceleration values ranged from $-1.5$ to $3.7$ m/s$^2$ at increments of $0.3$ m/s$^2$, while vehicle speeds varied from 0 to 33.5 m/s at increments of 0.3 m/s [13].

Generally, two types of mathematical models were investigated, nonlinear regression models and artificial neural network models. For the purposes of this study, the instantaneous fuel consumption, $F(v_i, a_i)$ (L/s), of an individual vehicle, can be expressed as:

$$F(v_i, a_i) = \exp\left(\sum_{j_1=0}^{3}\sum_{j_2=0}^{3} K_{j_1 j_2}(v_i)^{j_1}(a_i)^{j_2}\right), \qquad (4.3)$$

where $v_i$ and $a_i$ are the speed (m/s) and acceleration (m/s$^2$) of the vehicle at time $i$, respectively; $j_1$ and $j_2$ are the power indexes; $K_{j_1 j_2}$ are constant coefficients that can be found in Table 4.1 [19].

**Table 4.1**   Coefficients of the VT-micro model

| $K_{j_1 j_2}$ | $j_2 = 0$ | $j_2 = 1$ | $j_2 = 2$ | $j_2 = 3$ |
|---|---|---|---|---|
| $j_1 = 0$ | −7.537 | 0.4438 | 0.1716 | −0.0420 |
| $j_1 = 1$ | 0.0973 | 0.0518 | 0.0029 | −0.0071 |
| $j_1 = 2$ | −0.003 | −7.42E−04 | 1.09E−04 | 1.16E−04 |
| $j_1 = 3$ | 5.3E−05 | 6E−06 | −1E−05 | −6E−06 |

#### 4.2.2.2  The VSP Model

The concept of vehicle specific power (VSP) is a formalism used in the evaluation of vehicle emissions. Vehicle specific power is defined as the instantaneous power per unit mass of the vehicle [14]. The instantaneous power generated by the engine is used to overcome the rolling resistance and aerodynamic drag and to increase the kinetic and potential energies of the vehicle [14], so VSP is described as:

$$\text{VSP} = \frac{\text{Power}}{\text{mass}} = \frac{\frac{d}{dt}\left(E_{\text{kinetic}} + E_{\text{potential}}\right) + F_{\text{rolling}} \cdot v + F_{\text{aerodynamic}} \cdot v}{m}, \quad (4.4)$$

where $E_{\text{kinetic}}$ is the kinetic energy; $E_{\text{potential}}$ is the potential energy, $F_{\text{rolling}}$ is the rolling resistance force; $F_{\text{aerodynamic}}$ is the aerodynamic resistance force; $v$ is the vehicle speed; and $m$ is the vehicle mass. More specifically, it equals the product of speed and an equivalent acceleration, which includes the effects of roadway grade and rolling resistance, plus a term for aerodynamic drag which is proportional to the cube of the instantaneous speed [14], as described by:

$$\text{VSP} = \frac{\text{Power}}{\text{mass}} = \frac{\frac{d}{dt}\left(\frac{1}{2}m \cdot (1 + \varepsilon_i) \cdot v^2 + mgh\right) + C_R mg \cdot v + \frac{1}{2}\rho_a C_D A(v + v_w)^2 \cdot v}{m},$$
$$(4.5)$$

and hence,

$$\text{VSP} = v \cdot (a \cdot (1 + \varepsilon_i) + g \cdot \text{grade} + g \cdot C_R) + \frac{1}{2}\rho_a \frac{C_D \cdot A}{m}(v + v_w)^2 \cdot v, \quad (4.6)$$

where $v$, $m$ as described above, given in m/s and kg, respectively; $a$ is the vehicle acceleration (m/s²); $\varepsilon_i$[1] is the "mass factor," which is the equivalent translational mass of the rotating components (wheels, gears, shafts, etc.) of the powertrain; $h$ is the altitude of the vehicle; grade[2] [14]. However, for the purposes of this study, $\sin(\tan^{-1}(\text{grade}))$ was used.) is the vertical rise divided by the slope length; $g$ is the gravitational acceleration (9.81 m/s²); $C_R$[3] is the coefficient of rolling resistance (dimensionless); $C_D$ is the drag coefficient (dimensionless); $A$ is the frontal area of the vehicle; $\rho_a$ is the ambient air density (1.207 kg/m³ at 20 °C); $v_w$ is the headwind into the vehicle. The last term of Eq. 4.6, the load due to aerodynamic drag, depends on the factor $(C_D \cdot A/m)$ which is different for each specific vehicle model. An estimate was done based on the bibliography and was set equal to 0.0005. Thus, the

---

[1] Typical values of $\varepsilon_i$ for a manual transmission are 0.25 in 1st gear, 0.15 in 2nd gear, 0.10 in 3rd gear, 0.075 in 4th gear, etc. Finally, $\varepsilon_i$ was set equal to 0.1 [14].

[2] Rigorously $\sin(\tan^{-1}(\text{grade}))$ should be used instead of grade, but the error of this approximation is small (less than 1% relative error for grades below 14%.

[3] The value of $C_R$ depends on the road surface and tire type and pressure, with a small dependence on vehicle speed, with typical values ranging from 0.0085 to 0.016, so a value of 0.0135 has been used [14].

vehicle specific power, after calculations, is given in W/kg, as:

$$\text{VSP} = v \cdot (1.1 \cdot a + 9.81 \cdot \text{grade} + 0.132) + 3.02 \cdot 10^{-4}(v + v_w)^2 \cdot v. \quad (4.7)$$

For the purposes of this study, the following form was used:

$$\text{VSP}_i = v_i \cdot (1.1a_i + 9.81g + 0.132) + 3.02 \cdot 10^{-4}v_i^3, \quad (4.8)$$

where $\text{VSP}_i$ is the instantaneous vehicle specific power (W/kg); $v_i$ and $a_i$ are the speed (m/s) and acceleration (m/s$^2$) of the vehicle at time $i$, respectively; $g$ denotes the road grade given as mentioned previously.

To perform the energy characterization of a vehicle, a portable laboratory was used to measure fuel consumption, pollutant emissions, and vehicle dynamics under on-road conditions of 14 conventional vehicles and 5 hybrid vehicles. For each second of driving, according to the power demand resulting from the vehicle specific power $\text{VSP}_i$ mentioned above, the correspondent VSP mode was calculated. Using the data collected on-road, a general trend of fuel consumption as a function of VSP mode was observed, which was defined by 6 coefficients adjustable from vehicle to vehicle according to the certification inputs [15]. As a result, the instantaneous fuel consumption is expressed as a function of vehicle specific power, $\text{VSP}_i$ (g/s), as:

$$F(v_i, a_i) = F(\text{VSP}_i) = \begin{cases} f, & \text{if VSP}_i < -10 \\ \alpha\text{VSP}_i^2 + b\text{VSP}_i + c, & \text{if } -10 \le \text{VSP}_i \le 10 , \\ m\text{VSP}_i + d, & \text{if VSP}_i > 10 \end{cases} \quad (4.9)$$

where $\alpha = 1.98\text{E}{-}03$, $b = 3.97\text{E}{-}02$, $c = 2.01\text{E}{-}01$, $d = 2.48\text{E}{-}03$, $f = 2.48\text{E}{-}03$, and $m = 7.93\text{E}{-}02$ are coefficient values corresponding to one of the testing vehicles that were used [15]. To obtain the results in L/s, the instantaneous fuel consumption, $F(v_i, a_i)$ (g/s), is divided by the fuel density. For the purposes of this work, we assume only diesel vehicles, and hence, the oil density $\rho$ is estimated around 850 g/L.

### 4.2.2.3 The ARRB Model

Australian road research board (ARRB) model is an instantaneous fuel consumption model suitable for determining the incremental effects on fuel consumption resulting from changes in traffic management [16]. The model relates fuel consumption to the fuel to maintain engine operation and to the energy consumed (word done) in providing tractive force to the vehicle.

A power-based model was proposed that could relate the instantaneous fuel consumption to the instantaneous power demand experienced by the vehicle, using a simple linear relation [20]. However, the validation of this power model was not sufficient for the use of the model in the detailed assessment of the impacts of proposed

traffic management schemes. Using data collected from carefully controlled on-road acceleration, deceleration, and steady-speed fuel consumption tests, it was demonstrated that the power model gave adequate estimates of fuel consumption over trip segments of at least 60 s duration, as well as during cruise and slow-to-medium accelerations (mean errors generally less than 5%) [21]. On the other hand, during hard accelerations, fuel consumption was significantly underestimated, with mean errors of up to 20% depending on the acceleration and final speed [16]. Therefore, an extension (ARRB model) of the power model was presented, improving the accuracy of estimated fuel consumption, especially during hard accelerations [22].

For the purposes of this work, ARRB fuel consumption model can be expressed as the following simple polynomial function of instantaneous speed and acceleration, given in mL/s, as described by:

$$F(v_i, a_i) = \beta_1 + \beta_2 v_i + \beta_3 v_i^2 + \beta_4 v_i^3 + \gamma_1 v_i a_i + \gamma_2 v_i \big(\max(0, a_i)^2\big), \quad (4.10)$$

where $v_i$ and $a_i$ are the speed (m/s) and acceleration (m/s$^2$) of the vehicle at time $i$, respectively; $\beta_1 = 0.666$; $\beta_2 = 0.019$; $\beta_3 = 0.001$; $\beta_4 = 0.00005$; $\gamma_1 = 0.12$; $\gamma_2 = 0.058$. These parameters were calibrated using a Cortina test car, so that the model will accurately estimate the contribution of each energy component to fuel consumption [16].

#### 4.2.2.4 Fuel Consumption Estimation

To obtain meaningful results from the fuel consumption models, the vehicle's fuel consumption, $F_c$ (L/100 km), results by integrating the instantaneous fuel consumption, $F(v_i, a_i)$ (L/s), and dividing it by the distance covered which corresponds to the integration of the instantaneous speed over time. A factor of $10^{-5}$ is applied to the denominator so that the results are available in L/100 km, given by:

$$F_c = \frac{\int_0^T F(v_i, a_i)dt}{10^{-5} \cdot \int_0^T v dt}, \quad (4.11)$$

where $F(v_i, a_i)$ is the instantaneous fuel consumption of the various models, given in L/s; $v$ is the instantaneous speed (m/s); $dt$ is the time interval (s) between consecutive measurement points; $T$ denotes the total duration (s) of the travel period.

### *4.2.3 Experimental Campaigns*

#### 4.2.3.1 Ispra-Vicolungo

The first campaign was conducted in the first quarter of 2019, involving three days of car-following testing, on a section of Autostrada A26[4] between Ispra and Vicolungo, in northern Italy. The testing was performed with five ACC-equipped vehicles of various brands and models, driving in a car-platoon formation, in a 124.6 km round trip. Tests were scheduled for non-peak hours to minimize interference from other road users, such as cut-in behaviors. This real-world experiment aimed to collect driving data under actual traffic conditions in real-world scenarios.

Data acquisition was performed in binary format from the U-blox M8 devices,[5] with one device installed per vehicle. The acquired data had approximately a sampling frequency of 3–5 Hz, so cubic splines interpolation was implemented to achieve a 10 Hz frequency. GNSS receivers were configured to collect signals from both GPS and Galileo,[6] with the ability to process up to 16 satellite signals, enabling a good performance. The average horizontal accuracy reported by the receivers was less than 50 cm. GNSS active antennas were mounted on the roof of the cars, to ensure maximum satellite visibility and avoid signal attenuations from the body of the vehicles. At each time instant, the geographic coordinates (latitude, longitude, and altitude) of the vehicles were recorded. These coordinates were then transformed into a local East, North, and Up (ENU) Cartesian reference frame. Also, outliers were filtered using typical moving average postprocessing; big noisy parts have been removed from the dataset. Additional antennas were positioned to the front bumper of each vehicle to estimate the inter-vehicle distances. First, the instantaneous inter-vehicle distances are calculated based on position data, and then, these measurements are corrected based on computing bumper-to-bumper distances, by subtracting the leader's antenna-back bumper distance and the follower's antenna-front bumper distance.

The leader was instructed to drive manually and perform occasional random decelerations and accelerations over the desired speed. The followers, whenever possible, were driving with ACC systems enabled, apart from the last day when manual driving situations were tested. Therefore, to investigate the impact of both driving behaviors, the last day of the experimental campaign was the most appropriate for the purposes of this work. Specifically, on the southbound (SB) route (from Ispra to Vicolungo) of the trip, all vehicles were operated by human drivers. On the contrary, on the northbound (NB) route, the followers adopted ACC driving to regulate the longitudinal speed and the inter-vehicle distance with the minimum distance setting selected, while the leader and the last follower, whose drivers were respectively the same during the trip, were always human-driven. Also, a fixed vehicle order was adopted during the whole trip. Table 4.2 summarizes some of the vehicle specifications.

---

[4] Autostrada A26 is a motorway in the northwestern Italian regions of Liguria and Piedmont.

[5] https://www.u-blox.com/en/product/evk-8evk-m8.

[6] The European Global Navigation Satellite System (GNSS) receiver.

**Table 4.2**  Vehicle specifications for Ispra-Vicolungo campaign

|     | Vehicles | Max power (kW) | Engine size (cc) | Top speed (km/h) | Model year |
|-----|----------|----------------|------------------|------------------|------------|
| C1  | Mitsubishi SpaceStar | 59 | 1193 | 173 | 2018 |
| C2  | Ford S-Max | 110 | 1997 | 196 | 2018 |
| C3  | Peugeot 3008 GT Line | 130 | 1997 | 208 | 2018 |
| C4  | KIA Niro | 77.2 | 1580 | 172 | 2019 |
| C5  | Mini Cooper | 100 | 1499 | 210 | 2018 |

### 4.2.3.2   AstaZero Test Track

The second campaign was conducted in the second quarter of 2019, involving two days of car-following testing on the rural road of the AstaZero test track in Sweden. The testing was performed with five ACC-equipped vehicles, from four different makes (all different models), driving in a car-platoon formation. AstaZero's rural road is approximately 5.7 km long, half is designed for speeds around 70 km/h and a half for speeds around 90 km/h; however, its elevation profile is quite flat.

Trajectory data acquisition was performed with an inertial navigation system, the RT-Range S multiple target ADAS measurements solution by Oxford Technical Solutions Company, with a differential GNSS accuracy. The differential GNSS system ensures precision of 2 cm/s in the speed and 2 cm in the positioning measurements. This acquiring system provided a frequency of more than 100 Hz, so downsampling was applied to achieve a 10 Hz frequency, enough for capturing the vehicle dynamics in the platoon.

The experiments were organized in laps, containing five vehicles in a platoon formation. In all the tests, the leading vehicle was the same, and it was driven with the ACC system enabled to avoid noisy fluctuations around the desired speed due to manual maneuvers. In general, two different car-following patterns were applied for the following vehicles, a) car-platoon with constant speed, and b) car-platoon with the performance of perturbations (deceleration to a new desired speed) from an equilibrium point. For the second pattern, a radio-based communication between the drivers of the first and last vehicles ensured that the speed of the last vehicle was stable at the desired speed, and therefore, the car-platoon was close to an equilibrium state, before applying a new perturbation. Each perturbation was triggered by the driver by setting the desired speed of the ACC system to a new lower desired speed value. Consequently, the vehicle decelerates autonomously, and when the new desired speed is reached, the driver resets the desired speed to the previous setting. The duration of the perturbation is automatically adjusted based on the deceleration strategy applied by the controller. This procedure was selected to perform the different perturbations in a controlled way, and it resembles the way that vehicles with the ACC systems enabled behave on-road. For safety reasons, in each lap, the desired speeds were fixed to 13.9–16.7 m/s along the curves and to 25–27.8 m/s on the straight parts. Followers

**Table 4.3** Vehicle specifications from AstaZero campaign

|    | Vehicles        | Max power (kW) | Engine size (cc) | Top speed (km/h) | Model year |
|----|-----------------|----------------|------------------|------------------|------------|
| C1 | Audi A8         | 210            | 2967             | 250              | 2018       |
| C2 | Audi A6         | 150            | 1968             | 246              | 2018       |
| C3 | BMW X5          | 195            | 2993             | 230              | 2018       |
| C4 | Mercedes A Class| 165            | 1991             | 250              | 2019       |
| C5 | Tesla Model 3   | 150            | –                | 210              | 2019       |

were driving with ACC enabled, with the minimum distance setting selected, apart from two laps where manual driving situations were tested. To investigate the impact of ACC driving behavior compared to the human one, the two most suitable parts of AstaZero's database were selected for the assessment. The first part included only human driving vehicles except the first one, while the second one involved only vehicles with the ACC systems enabled. In addition, the same five vehicles were used, in the same fixed order. Table 4.3 summarizes some of the vehicle specifications.

## 4.3 Results and Discussion

This section employs several data analysis techniques to present the obtained results from the application of four energy demand and fuel consumption models (see Sects. 2.1 and 2.2) to the two experimental car-following campaigns presented in Sect. 2.3. The impact of ACC on tractive energy and fuel consumption is assessed from individual and platoon perspectives. Vehicles in the same platoon are experiencing quite similar road and traffic conditions but with totally different specifications. To isolate the driving behavior as the only possible contributor to tractive energy and fuel consumption differences, a scaling technique is employed to normalize heterogeneous vehicle specifications and road and traffic conditions. Specifically, this heterogeneity is handled by assuming that the same default values for the vehicle's road load coefficients and mass, among the various energy and fuel consumption models, are used for the whole platoon (platoon normalization).

### 4.3.1 Ispra-Vicolungo

The first experimental campaign consisted of five vehicles in a platoon formation, and was divided into two trajectory paths, one going from Ispra to Vicolungo (southbound route) and another returning back (northbound route), using the same vehicles in a fixed order during the whole trip (third day of the experiments). On the southbound route, all vehicles in the platoon were operated by human drivers, while on the

northbound route, the followers enabled the ACC systems. The first and the last vehicles were human-driven throughout the whole trip.

#### 4.3.1.1 Energy Consumption

The tractive energy values of the vehicles sharing the same platoon are compared, provided that all vehicles share the same specifications as those of their leader (platoon normalization). Figure 4.1 presents the obtained results from the campaign in Italy. Figure 4.1i displays the tractive energy impact of human and ACC driving behavior inside the platoon. The figure reveals a tendency for upstream energy propagation in the platoon with ACC systems enabled (northbound route). Specifically, the tractive energy values of the ACC followers (C2, C3, and C4) tend to consecutively increase, in contrast to the tractive energy values that their human counterparts achieve in the southbound route. Therefore, ACC systems seem to be less energy efficient than human-driven vehicles from a platoon perspective.
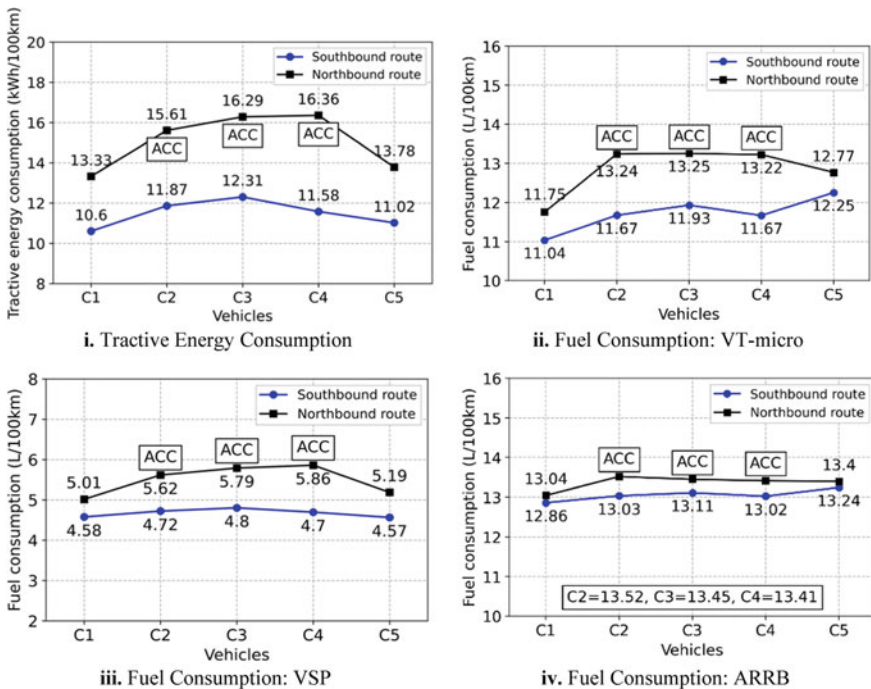


**Fig. 4.1** Energy and fuel consumption models (Ispa-Vicolungo)

#### 4.3.1.2 Fuel Consumption

The impact of ACC systems on fuel consumption inside the platoon is examined using the three independent fuel consumption models, as illustrated in Fig. 4.1. The results are given in (L/100 km). As can be seen, quite the same tendency is revealed among the various fuel consumption models, regarding the ACC driving behavior. More precisely, the findings of the VT-micro model reveal a strong fuel consumption amplification by the first ACC participant (C2) inside the platoon (northbound route), with the rest of them (C3, C4) maintaining the values on high levels relative to those that the human counterparts achieve in the southbound route. Additionally, the VSP model reveals quite similar results to the energy consumption model, regarding both ACC and human driving behaviors, showing the same exact tendency for fuel consumption propagation upstream of the platoon. On the contrary, the last human counterpart (C5) in the northbound route reveals a relatively downward value trend, in both VT-micro and VSP models, trying to absorb the fuel consumption propagations occurring upstream of the platoon from the ACC participants. The same behavior is also detected in the findings of tractive energy consumption, mentioned above. On the other hand, both driving modes seem to achieve very small value fluctuations showing almost flat fuel consumption profiles in the case of ARRB model, which seems to be a more conservative model. Finally, the value ranges among the three models seem to differ significantly, with the VSP model showing the largest deviations. Generally, ACC systems tend to increase fuel consumption inside the platoon in all three fuel consumption models and hence are less efficient compared to human-driven vehicles.

### 4.3.2 AstaZero

In this experimental campaign, a five-vehicle platoon was involved with the leading vehicle being always under ACC driving operation. Specifically, in the first phase, the following vehicles were operated by human drivers, while in the second one, all the vehicles adopted ACC driving. Finally, the same vehicles, in the same fixed order, were used in both parts.

#### 4.3.2.1 Energy Consumption

Figure 4.2 presents the obtained results from the AstaZero test track. As can be seen in Fig. 4.2i, the tractive energy values are amplified upstream of the platoon when ACC systems are enabled, especially for the last participants (C3, C4, and C5). On the other hand, human-driven vehicles reveal a more constant behavior with very small variations in tractive energy values. Consequently, the present results verify the above findings from the first experimental campaign in Italy, proving that ACC systems end up being more "energy-hungry."
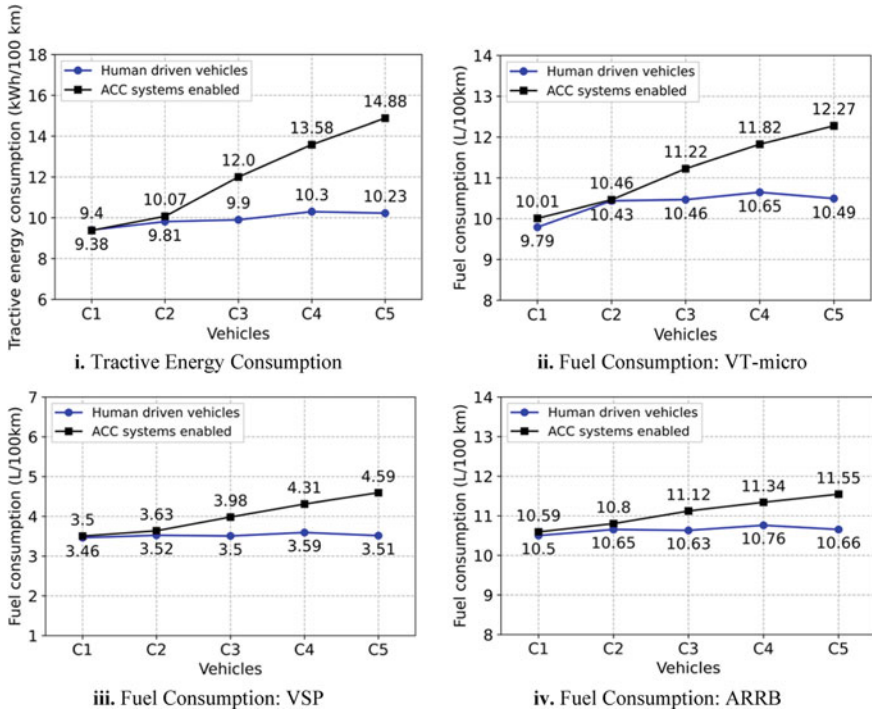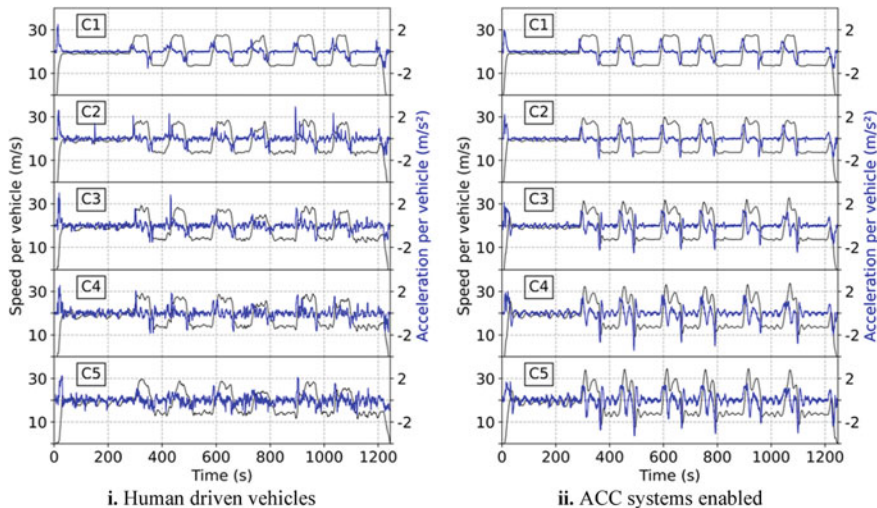
**Fig. 4.2** Energy and fuel consumption models (AstaZero)

#### 4.3.2.2 Fuel Consumption

In terms of fuel consumption, a clear upstream fuel consumption amplification by the ACC participants inside the platoon is detected among all three models, as shown in Fig. 4.2. On the contrary, the human counterparts seem to achieve very small value fluctuations showing a noticeably invariable behavior. The value ranges among the three fuel consumption models seem to differ again, with the VSP model showing quite unexpectedly small values. Eventually, the findings from both energy and fuel consumption models seem to be in total agreement with the above findings, indicating once again that the ACC systems turn out to be less energy efficient from a platoon perspective.

### 4.3.3 Discussion

Generally, the findings reveal that ACC participants cannot reduce fuel and energy consumption inside the platoon, tending to be more "energy-hungry" than human-driven vehicles and hence less energy efficient from a platoon perspective. Both

**Fig. 4.3** Speed/acceleration profiles (AstaZero)

experimental campaigns investigated, using four independent energy and fuel consumption models, seem to agree with this statement.

As mentioned in Sect. 4.1, ACC systems can automatically adjust the vehicle's speed by accelerating or decelerating it, to maintain a constant predefined time-gap with the vehicle in front or to reach the predefined desired speed. Figure 4.3 illustrates the speed and acceleration profiles of each testing vehicle, separately, taken from the second experimental campaign that was held on the rural road of AstaZero test track. As shown in the second subfigure on the right, ACC systems operate in a stricter way than human drivers do. More specifically, ACC participants reveal strong and sharp accelerations with several peaks and variations in the speed profile, especially when moving upstream the platoon (C3, C4, and C5), while human counterparts reveal smaller fluctuations around the equilibrium points, regarding speed and acceleration.

As a result, the way that ACC systems operate under car-following situations seems to affect the energy impact of the ACC participants inside the platoon. All the models presented in Sect. 4.2 estimate energy demand and fuel consumption, mainly, as functions of speeds and accelerations. Hence, there are plenty of peaks and spikes appearing in both speed and acceleration profiles when ACC systems are enabled, which could possibly affect their energy impact. The findings seem to verify the above hypothesis that the steeper points and spikes appear in the speed and acceleration profiles the greater fuel and energy consumption is.

Additionally, in Fig. 4.4 are presented two random perturbation events from the AstaZero campaign, which occurred between the same speeds for both driving modes. As previously mentioned, the ACC participants reveal several peaks and steep variations in the speed profile (as well as in the acceleration profile), especially when moving upstream of the platoon, as illustrated in Fig. 4.3ii. In the left subfigure,
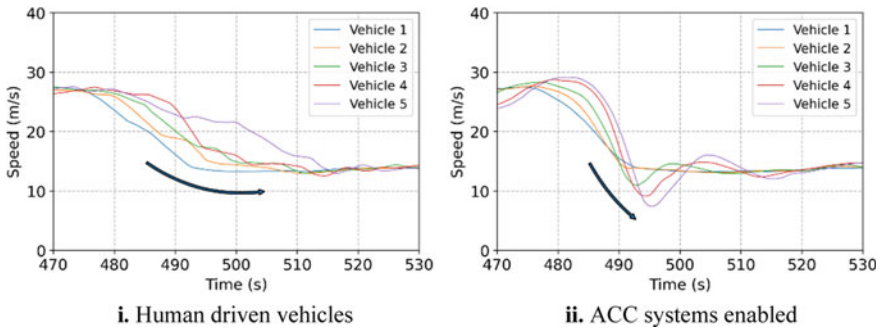
**Fig. 4.4** Speed overshoots (AstaZero)

the speed variations of the leader are not amplified through the human participants. However, in the second subfigure, ACC followers significantly enlarge their leader's speed perturbation, revealing large speed overshoots amplified upstream the platoon. These black curved arrows indicate the stable car-following behavior of human drivers (Fig. 4.4i) and the string instability that ACC participants cause (Fig. 4.4ii).

String stability is achieved in a platoon when the last following vehicle dissolves the perturbation imposed by the leading vehicle [23]. In other words, string stability means any nonzero position, speed, and acceleration errors of an individual vehicle in a string do not amplify when they propagate upstream [24]. The string stability of a platoon of five ACC-equipped vehicles under several conditions in the AstaZero proving ground was investigated, and the results show that in all conditions, ACC systems led to string unstable platoons [25].

Therefore, this string instability that ACC systems reveal could negatively affect their energy impact. Without loss of generality, a correlation between string stability and energy and fuel consumption seems to exist, with speed overshoots propagating upstream being proportional to the upstream amplification of energy and fuel consumption inside the platoon. Of course, this relation should be studied across the complete operational domain and under all possible conditions, to obtain meaningful and solid results.

Also, as it was previously mentioned, the last human participant (C5) in the northbound route of the first experimental campaign revealed a relatively downward value trend among the various fuel and energy consumption models, trying to absorb the energy propagation that occurred upstream of the platoon. Figure 4.5 depicts a random perturbation event during real-world conditions in the motorway of Autostrada A26 in Italy. The findings reveal that the last follower (C5) absorbs the speed overshoots propagating upstream the platoon. A possible explanation could be that human drivers can detect decelerations occurring 2–3 vehicles downstream of the platoon and hence responding in a more polite way. Therefore, this tendency for absorbing the perturbations propagating upstream of the platoon could be related to the lower energy and fuel consumption values achieved by the last participant.

**Fig. 4.5** Speed overshoots
with ACC systems enabled
(Ispra-Vicolungo)
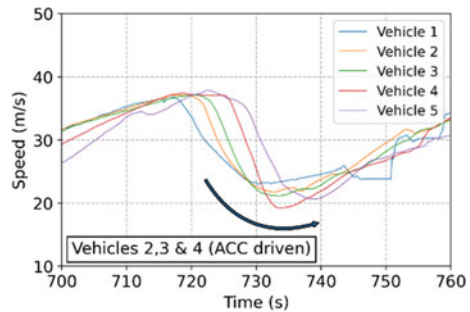


In addition, it is worth mentioning that another possible cause of string instability inside a platoon with ACC participants could be the road gradient. Several altitude changes are observed in the elevation profile of the Autostrada A26 motorway in Italy, since it is located at the foot of the Alps Mountains, which could significantly affect the way that ACC controllers operate under car-following situations.

More specifically, if we assume a vehicle with an ACC system enabled, under steady-state conditions with a constant predefined speed, an altitude increase would require additional work from the controller to reach the predefined speed. In this effort, trying to counterbalance the impact of the road grade, the controller ends up overshooting. In a similar way, as the altitude decreases, the controller undershoots reaching a lower speed than the desired one. In both cases, oscillations are generated around the predefined speed directly affecting the followers (assume ACC participants). These oscillations propagating upstream of the platoon could lead to string instability and hence affect the energy impact of ACC systems as it was mentioned previously. Even for slight perturbations derived by variability in the road gradient, string instability can be observed, raising concerns about potential consequences in traffic flow as the penetration rate of ACC systems is rapidly increasing [25].

However, as it turns out, ACC systems do not generally fail inside a platoon. More precisely, Figs. 4.6 and 4.7 provide an estimation of time/space-gap distributions for both experimental campaigns. The computation of time-gaps between two vehicles inside the platoon was performed by dividing the obtained space-gaps (IVS) between two vehicles with the speed of the following vehicle. Space-gaps were already estimated and hence, available in the two experimental datasets. As can be seen (see Figs. 4.6 and 4.7), the time- and space-gaps are smaller (in absolute values) with ACC engaged and better distributed compared to human drivers. Provided that the time-gaps are more or less constant with ACC engaged, we conjecture that the commercial ACC system in the cars in Table 4.3 employs a constant time-gap policy. However, the core functionality (controller type and its parameters) is not publicly available, so any conclusions must be drawn with caution.

This positive result for the ACC drivers is attributed to the ACC controller. It highlights that commercial ACC controllers (despite the criticism to their negative impact concerning traffic flow and stability) deliver some improvements. Actually, the improvements to be expected from their design and controller synthesis (e.g.,
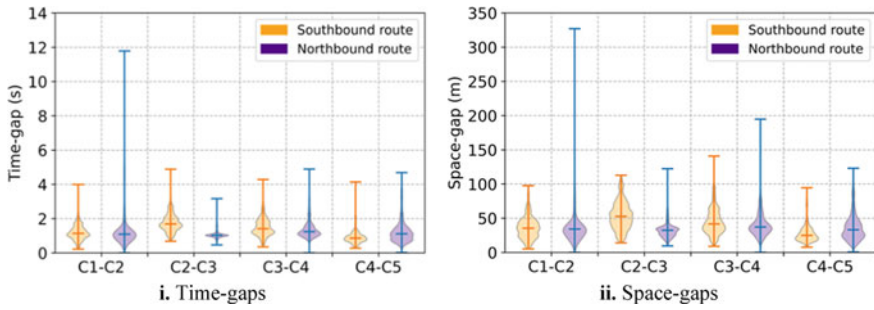
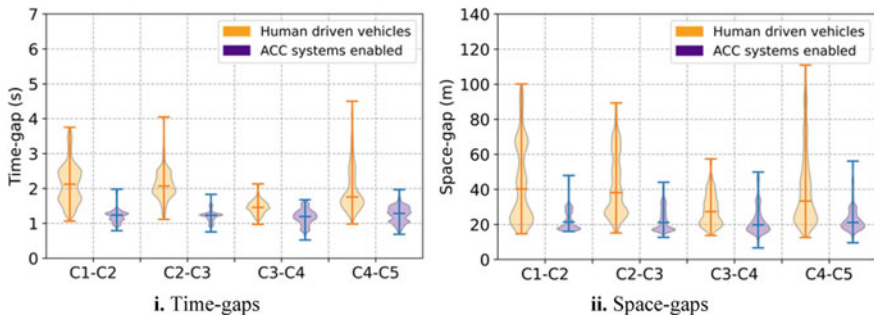**Fig. 4.6** Time-gap/space-gap distributions (Ispra-Vicolungo)



**Fig. 4.7** Time-gap/space-gap distributions (AstaZero)

constant time-gap), i.e., to keep constant and safe space/time-gaps. However, it is well known that constant spacing (space-gap) policies lead to string unstable platoons of vehicles [26–28], while constant time-gap policies are string stable for ACC vehicles without inter-vehicle connectivity [2, 4, 5, 29].

Another observation is related to the comparison of the same graphs (Figs. 4.6 and 4.7) for the two different campaigns (one took place in a public motorway network and the other in a protected test environment). In the protected environment of AstaZero, it seems that the improvements for the space/time-gaps are more evident and higher compared to the campaign in Italy. This is attributed to: (a) the employed vehicles (characteristics/specifications), (b) the environment (protected in AstaZero, so no inference with other cars and mixed heterogeneous traffic, a public motorway in Italy with mixed traffic and more disturbances). These observations also underline that ACC drivers in protected environments and campaigns might perform better but can be (ideally) tested in adverse environments.

Therefore, as it was previously mentioned, in both experimental campaigns, an upstream energy propagation was observed inside the platoon by the ACC participants, regarding both energy and fuel consumption, indicating that ACC systems are less efficient. However, the ACC participants succeed in maintaining a constant predefined time-gap between two consecutive vehicles, which is part of the ACC

logic and one of the requirements vehicle manufacturers need to fulfill. ACC distributions seem to be more accumulated around lower levels compared to human ones, especially in the AstaZero campaign, indicating that ACC systems are more efficient. It seems that the more efficient ACC systems are regarding their functional specifications, the less energy efficient tend to be. Consequently, a trade-off between time/space-gaps and fuel and energy consumption could exist, to eliminate high energy levels and achieve the desired safety, at the same time.

## 4.4   Conclusions and Outlook

This study assessed the energy impact of ACC systems under car-following conditions. The thematic focus was laid on investigations into energy demand and fuel consumption for human-driven and ACC-engaged vehicles in real-life experimental campaigns with a variety of vehicle specifications, propulsion systems, drivers, and road and traffic conditions. To this end, high-resolution empirical data from two experimental car-following campaigns were used. Then, energy demand and fuel consumption estimations were calculated by employing four independent models. The main findings of this study can be summarized as follows:

- ACC systems are less energy efficient, revealing a tendency for upstream energy propagation inside the platoon.
- Human counterparts adopt a more conservative and invariable energy behavior.
- ACC driving operation (strong accelerations, steep speeds, etc.) may negatively affect the energy impact of ACC systems under car-following conditions.
- ACC systems may lead to string instability failing to avoid an upstream energy amplification.
- Road gradient changes could create string instabilities in the traffic flow and may negatively affect the energy impact of ACC systems under car-following conditions.
- ACC systems succeed in delivering a constant time-gap policy, between two consecutive vehicles, at lower levels than human drivers do.

It should be noted that there is an agreement for both campaigns (one conducted in a public highway and the other in a protected test site) and for four independent models in terms of tractive energy and fuel consumption footprint (human drivers are more efficient compared to the ACC drivers), despite the different data acquisition methods employed and the differences in the design and execution of the experimental campaigns.

Finally, it should be highlighted that the more efficient ACC systems are regarding their functional specifications, the less energy efficient tend to be. Consequently, commercial ACC systems must be designed to realize a trade-off between functional specifications in terms of time/space-gaps and tractive energy and fuel consumption. This will ideally eliminate high energy levels and achieve the desired safety features of commercial ACC systems.

Further study should focus on:

- The trade-off between time/space-gaps and fuel and energy consumption of ACC systems driving in a car-platoon formation, toward a more complete picture of the fundamental relations between the several requirements vehicle manufacturers need to fulfill.
- The correlation between the leader's and the follower's driving profile (i.e., speed-acceleration), see, e.g., [11]. Such analysis would be useful to unveil how strong is the bond between the (free) leader and ego vehicles in a platoon (whose mission is to ensure safety and keep constant headways).
- The design and synthesis of ACC systems with safe and eco-driving instructions. However, this might lead ACC drivers to brake at longer safety margins for safety and energy savings toward eco-driving.

Finally, the results presented in this study and in the relevant literature might be biased toward the acquisition method used in different experimental campaigns. Thus, additional analysis for various energy and fuel consumption models using empirical data from other experimental campaigns employing different acquisition methods can be conducted to shed some light on the energy footprint of human and ACC drivers.

# References

1. SAE International: Taxonomy and Definitions for Terms Related to Driving Automation Systems for On-Road Motor Vehicles (2021)
2. Ioannou, P.A., Chien, C.C.: Autonomous intelligent cruise control. IEEE Trans. Veh. Technol. **42**, 657–672 (1993)
3. Swaroop, D.: String stability of interconnected systems: an application to platooning in automated highway systems (1997)
4. Swaroop, D., Hedrick, J.K.: String stability of interconnected systems. IEEE Trans. Autom. Control **41**, 349–357 (1996)
5. Liang, C.-Y., Peng, H.: Optimal adaptive cruise control with guaranteed string stability. Veh. Syst. Dyn. **32**, 313–330 (1999)
6. Shi, X., Yao, H., Liang, Z., Li, X.: An empirical study on fuel consumption of commercial automated vehicles. Transp. Res. Part D Transp. Environ. **106**, 103253 (2022)
7. Li, S., Li, K., Rajamani, R., Wang, J.: Model predictive multi-objective vehicular adaptive cruise control. IEEE Trans. Control Syst. Technol. **19**, 556–566 (2011)
8. Dvorkin, W., King, J., Gray, M., Jao, S.: Determining the Greenhouse Gas Emissions Benefit of an Adaptive Cruise Control System Using Real-World Driving Data, p. 9 (April 2019)
9. Ciuffo, B., Mattas, K., Makridis, M., Albano, G., Anesiadou, A., He, Y., Josvai, S., Komnos, D., Pataki, M., Vass, S., Szalay, Z.: Requiem on the positive effects of commercial adaptive cruise control on motorway traffic and recommendations for future automated driving systems. Transp. Res. Part C Emerg. Technol. **130**, 103305 (2021)
10. Knoop, V.L., Wang, M., Wilmink, I., Hoedemaeker, D.M., Maaskant, M., der Meer, E.-J.V.: Platoon of SAE Level-2 automated vehicles on public roads: setup, traffic interactions, and stability. Transp. Res. Rec. **2673**, 311–322 (2019)
11. He, Y., Makridis, M., Fontaras, G., Mattas, K., Xu, H., Ciuffo, B.: The energy impact of adaptive cruise control in real-world highway multiple-car-following scenarios. Eur. Transp. Res. Rev. **12** (December 2020)

12. Ehsani, M., Gao, Y., Gay, S.E., Emadi, A.: Modern Electric, Hybrid Electric, and Fuel Cell Vehicles: Fundamentals, Theory, and Design, 3rd ed. CRC Press (2018)
13. Ahn, K.: Microscopic fuel consumption and emission modeling (1998)
14. Jiménez-Palacios, J.L.: Understanding and quantifying motor vehicle emissions with vehicle specific power and TILDAS remote sensing (1999)
15. Duarte, G.O., Gonçalves, G.A., Baptista, P.C., Farias, T.L.: Establishing bonds between vehicle certification data and real-world vehicle fuel consumption–a Vehicle Specific Power approach. Energy Convers. Manage. **92**, 251–265 (2015)
16. Akçelik, R., Biggs, D.C.: An energy-related model of instantaneous fuel consumption. Traffic Eng. Control **27**, 320–325 (1986)
17. Makridis, M., Fontaras, G., Ciuffo, B., Mattas, K.: MFC free-flow model: introducing vehicle dynamics in microsimulation. Transp. Res. Rec. **2673**, 762–777 (2019)
18. Rakha, H., Ahn, K., Trani, A.: Development of VT-Micro model for estimating hot stabilized light duty vehicle and truck emissions. Transp. Res. Part D Transp. Environ. **9**, 49–74 (2004)
19. Zegeye, S.K., Schutter, B.D., Hellendoorn, J., Breunesse, E.A., Hegyi, A.: Integrated macroscopic traffic flow, emission, and fuel consumption model for control purposes. Transp. Res. Part C Emerg. Technol, **31**, 158–171 (2013)
20. Post, K., Kent, J.H., Tomlin, J., Carruthers, N.: Fuel consumption and emission modelling by power demand and a comparison with other models. Transp. Res. Part A Gen. **18**, 191–213 (1984)
21. Akçelik, R., Biggs, D.C.: Validation of a power based model of car fuel consumption. Australian Road Research Board, Internal Report AIR 390-4 (1984)
22. Akçelik, R., Biggs, D.C.: Further work on modelling car fuel consumption. Australian Road Research Board, Internal Report AIR 390-10 (1985)
23. Monteil, J., Bouroche, M., Leith, D.J.: $L_2$ and $L_\infty$ stability analysis of heterogeneous traffic with application to parameter optimization for the control of automated vehicles. IEEE Trans. Control Syst. Technol. **27**, 934–949 (2019)
24. Lei, C., van Eenennaam, E.M., Klein Wolterink, W., Ploeg, J., Karagiannis, G., Heijenk, G.: Evaluation of CACC string stability using SUMO, Simulink, and OMNeT++. EURASIP J. Wirel. Commun. Netw. **2012**, 1–12 (2012)
25. Makridis, M., Mattas, K., Ciuffo, B., Re, F., Kriston, A., Minarini, F., Rognelund, G.: Empirical study on the properties of adaptive cruise control systems and their impact on traffic flow and string stability. Transp. Res. Rec. **2674**, 471–484 (2020)
26. Seiler, P., Pant, A., Hedrick, K.: Disturbance propagation in vehicle strings. IEEE Trans. Autom. Control **49**, 1835–1842 (2004)
27. Jovanovic, M.R., Bamieh, B.: On the ill-posedness of certain vehicular platoon control problems. IEEE Trans. Autom. Control **50**, 1307–1321 (2005)
28. Middleton, R.H., Braslavsky, J.H.: String instability in classes of linear time invariant formation control with limited communication range. IEEE Trans. Autom. Control **55**, 1519–1530 (2010)
29. Rajamani, R., Zhu, C.: Semi-autonomous adaptive cruise control systems. IEEE Trans. Veh. Technol. **51**, 1186–1192 (2002)